ADVANCED MATERIALS

www.advmat.de

Visualization Recording and Storage of Pressure Distribution through a Smart Matrix Based on the Piezotronic Effect

Xun Han, Weiming Du, Mengxiao Chen, Xiandi Wang, Xiaojia Zhang, Xiaoyi Li, Jing Li, Zhengchun Peng, Caofeng Pan, and Zhong Lin Wang**

Pressure sensors that can both directly visualize and record applied pressure/stress are essential for e-skin and medical/health monitoring. Here, using a WO_3-film electrochromic device (ECD) array (10 × 10 pixels) and a ZnO-nanowire-matrix pressure sensor (ZPS), a pressure visualization and recording (PVR) system with a spatial resolution of 500 μm is developed. The distribution of external pressures can be recorded through the piezotronic effect from the ZPS and directly expressed by color changes in the ECD. Applying a local pressure can generate piezoelectric polarization charges at the two ends of the ZnO nanowires, which leads to the tuning of the current to be transported through the system and thus the color of the WO_3 film. The coloration and bleaching process in the ECD component show good cyclic stability, and over 85% of the color contrast is maintained after 300 cycles. In this PVR system, the applied pressure can be recorded without the assistance of a computer because of the color memory effect of the WO_3 material. Such systems are promising for applications in human-electronic interfaces, military applications, and smart robots.

Pressure sensors are basic components of electrical skins, which are designed to comprehensively imitate human skin using electronic devices.[1] Other related applications that rely on pressure-sensitive components include medical/health monitoring,[2] robotics,[3] interactive control systems and artificial intelligence.[4] The resistance and capacitance of some pressure sensitive electronic devices can change with applied stresses.[5] Based on this, many excellent studies have been carried out to develop pressure sensors with high sensitivity and high resolution.[6] This research has led to achievements in large-scale pressure detection and visualization.[7] However, most of these detection systems need a computer to record signals from the pressure sensor in real time.[8] Thus, if the computer was disconnected when a certain pressure was applied to the system, the relevant signals would not be reproduced. In some special cases, such as in black boxes and when monitoring under extreme conditions, the circumstances do not permit the signals to be addressed at their first instance; it would be beneficial if the sensor device itself could "hold/keep" the pressure signals for a period of time. Few studies have reported on recording the pressure simultaneously using these devices. Pressure sensors that can record the pressure distribution with no assistance from a computer are therefore eagerly anticipated.

Here, we develop a pressure visualization and recording (PVR) system with a spatial resolution of 500 μm (50.8 dpi). This concept is realized through the development and integration of a ZnO-nanowire-matrix pressure sensor (ZPS), which undergoes the piezotronic effect, and a WO_3-film electrochromic device (ECD) array (10 × 10 pixels). Each pixel is connected to a certain group of ZnO nanowires on the top of the ZPS component through an Au electrode layer. The coloration and bleaching process in the ECD component showed good cyclic stability, and over 85% of the color contrast was maintained after 300 cycles. The distribution of external pressures can be recorded by the ZPS through the piezotronic effect and expressed directly by color changes on the ECD. Furthermore, this PVR system can independently record the external pressure distribution through the color memory effect of the WO_3 material.[9] Such systems are promising for applications in human-electronic interfaces, military applications, and smart robots.

The structure of the PVR system is schematically illustrated in **Figure 1**a. The system consists of a ZPS based on the

X. Han, W. Du, M. Chen, X. Wang, X. Zhang, X. Li, J. Li, Prof. C. Pan, Prof. Z. L. Wang
Beijing Institute of Nanoenergy and Nanosystems
Chinese Academy of Sciences
CAS Center for Excellence in Nanoscience
National Center for Nanoscience and Technology (NCNST)
Beijing 100083, P. R. China
E-mail: cfpan@binn.cas.cn; zhong.wang@mse.gatech.edu
Prof. Z. Peng
College of Optoelectronic Engineering
Shenzhen University
Shenzhen 518060, P. R. China
Prof. Z. L. Wang
School of Materials Science and Engineering
Georgia Institute of Technology
Atlanta, GA 30332-0245, USA

The ORCID identification number(s) for the author(s) of this article can be found under http://dx.doi.org/10.1002/adma.201701253.

DOI: 10.1002/adma.201701253

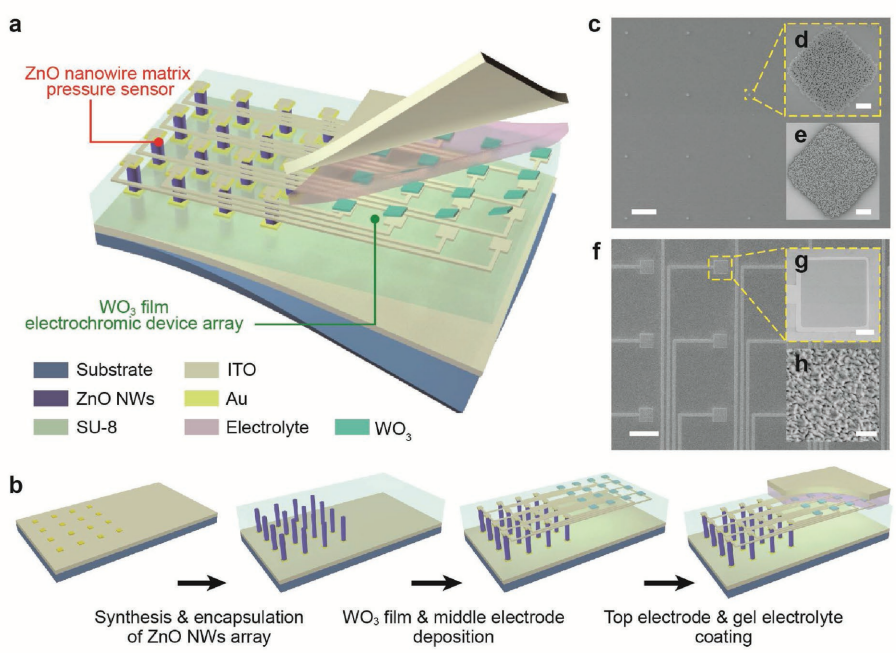

Figure 1. Structure and fabrication process of the PVR system. a) Schematic illustration of the structure of the PVR system. b) Schematic diagram showing the fabrication process of the PVR system. c) SEM image of the as-fabricated ZnO NW matrix before spin-coating a layer of SU-8 photoresist. The scale bar is 200 µm. Enlarged images of the ZnO NWs d) before and e) after spin-coating the SU-8 layer. The scale bars are both 5 µm. f) SEM image of the as-fabricated middle Au electrode and WO_3 film array. The scale bar is 200 µm. g) The WO_3 film deposited on the ITO electrode and h) its magnified view. The scale bars are 20 µm and 200 nm, respectively.

piezotronic effect and a WO_3-film ECD array. The ZPS was used for external pressure detection, and the ECD was used to simultaneously visualize and record the pressure distribution. Figure 1b outlines the fabrication process of the PVR system. The ZPS was fabricated first. An indium tin oxide (ITO) film was deposited on a pre-cleaned glass substrate as the bottom electrode. Sequentially, a patterned Au layer and a ZnO seed layer were precisely deposited in a 20 µm × 20 µm quadrant array with 480 µm intervals, and Schottky contacts were formed. Then, ZnO nanowires were synthesized on the top of the seed layer through a low-temperature hydrothermal method. The corresponding scanning electron microscopy (SEM) image is shown in Figure 1c. Thus, a resolution of 500 µm (50.8 dpi), determined by the ZnO nanowire matrix, was obtained for the ZPS component. To improve the stability under pressure, SU-8 photoresist was wrapped around the ZnO nanowire bunches. The last step in fabricating the ZPS component was the deposition of the top electrode layer. This layer is a key to connect the ZPS and the ECD (through the bottom electrode of the ECD), and thus it can be regarded as the linking electrode. Specially designed linking electrodes were fabricated to connect the ZPS and ECD by one nanowire bunch to one pixel, which provides a consistent spatial resolution. The WO_3-film array was then deposited on the patterned linking electrode to create pixels in the ECD array. The linking electrodes and WO_3 film were carefully characterized by SEM, as shown in Figure 1f. Next, the electrolyte was spin-coated on the WO_3-film array, followed by the final step of covering the ECD with ITO glass as the top electrode. Detailed fabrication processes can be found in the Experimental Section. Upon the application of strain, the current through the compressed areas in the ZPS will increase, which makes the corresponding pixels of the ECD array become darker. The dark color of these pixels can be retained for a period of time because of the coloration retention properties of the WO_3 film. Therefore, the applied pressure is visualized and recorded.

A variety of pressures were applied to introduce a piezopotential to tune the carrier transport process in the ZnO nanowires. The current–voltage (*I*–*V*) characteristics of a single pixel in the ZPS component were investigated and are summarized in **Figure 2**a. The output currents clearly increased with applied pressure under forward bias but remained almost unchanged under reverse bias. Furthermore, the sensitivity and stability of a single pixel in the ZPS component under various pressures were also investigated under a bias of +1 V. When the applied pressure was first increased and then decreased (0 to 70.42 to 0 MPa), the current response was stable. Pressure values with minor differences could also be distinguished in the current–time (*I*–*t*) curve in Figure 2b, indicating a satisfactory sensitivity.

The working principle of the piezotronic effect in the ZPS was illustrated by analyzing the energy band of the Au–ZnO–Au structure, as shown in Figure 2c–e. Mechanical straining creates piezoelectric polarization charges at the two ends of the nanowires, which respectively tune the local Schottky contacts either high or low depending on the sign of the local electrostatic charges.[10] Thus, the electric current to be transported through the entire device through the WO_3 layer is tuned, which changes the rate of the local electrochemical process, resulting in a tuning of the local color. Two Schottky

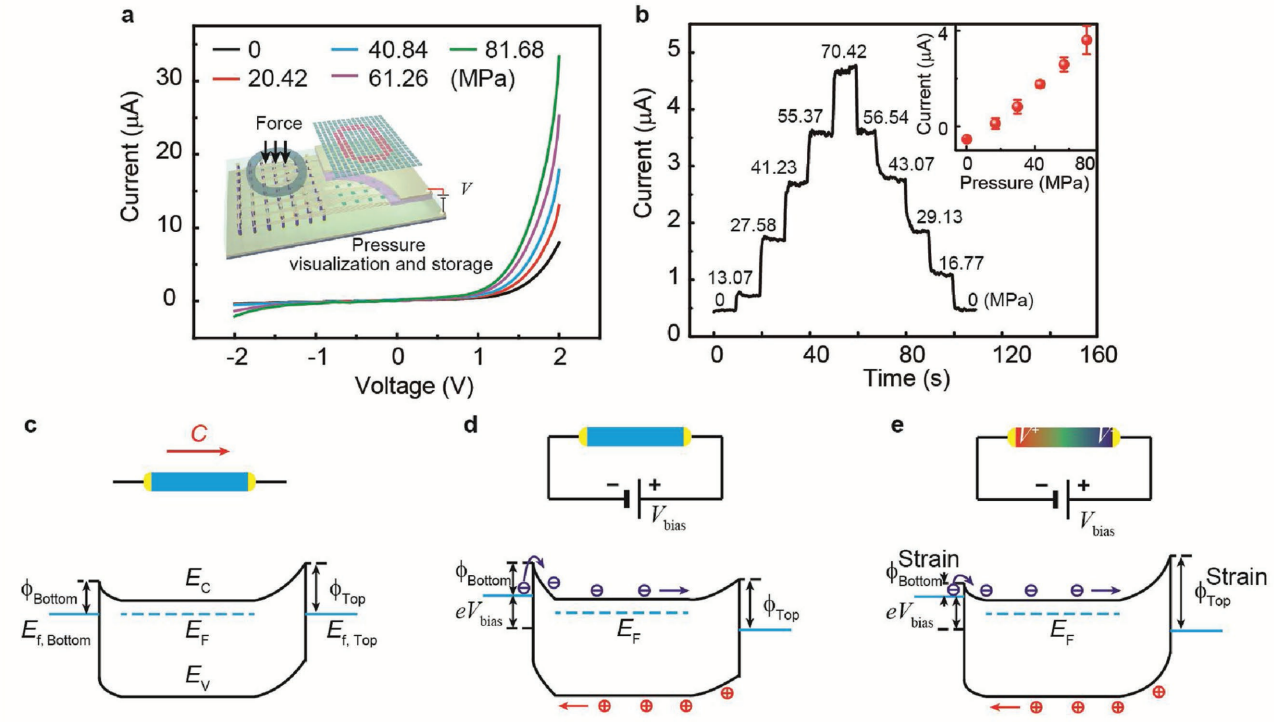

Figure 2. Piezotronic effect on pressure sensing and the working mechanism. a) *I–V* characteristics of a single ZnO NW pixel under various applied pressures. b) *I–t* characteristics of the ZnO NW pixel under various pressures to illustrate the stability and sensitivity at +1 V. The inset shows the current changes under external pressures at +1 V. Energy band diagrams of the ZnO NWs c) under strain-free conditions without an applied voltage bias, d) under strain-free conditions with a forward bias, and e) under compressive strain with a forward bias.

were contacts formed at the two ends of the ZnO nanowire between the Au electrode and the ZnO band edges, with two Schottky barrier heights (SBHs) of Φ_{bottom} and Φ_{top}, respectively (Figure 2c).[11] Under forward bias, the quasi-Fermi levels of the Au electrodes shifted. This shift mainly occurs at the Schottky contact with the bottom Au electrode, which is connected to the cathode and dominates the electronic transport process (Figure 2d). According to basic piezotronic theory, if the *c*-axis of a ZnO nanowire points to the top electrode, when compressive strain is applied along the nanowire, positive charges are created at the bottom contact to reduce the bottom SBH, and negative charges are introduced at the top contact to increase the top SBH (Figure 2e).[12] This leads to enhanced performance under forward bias, as shown in Figure 2a. On the other hand, the top SBH is large enough to neglect the introduced piezopotential, and thus with applied pressure, the current remains almost unchanged under reverse bias, as shown in Figure 2a.

For the integrated PVR system, a WO_3 film was selected as the functional material of the ECD array. The electrochromic properties of the ECD are shown in **Figure 3**. The as-deposited WO_3 film is amorphous[13] (Figure S1, Supporting Information), and the color of the WO_3 film can be changed from transparent to blue reversibly and persistently by the intercalation of electrons and small cations (such as H^+, Li^+, etc.).[14] The coloration and bleaching (intercalation/de-intercalation) process in Li^+ electrolyte can be expressed through the following reversible reaction[15]

$$WO_3 + xe^- + xLi^+ \leftrightharpoons Li_xWO_3 \quad (1)$$

Cyclic voltammograms of the WO_3 thin film were recorded at three different scan rates (20, 50, and 100 mV s^{-1}) in 1 M H_2SO_4, as shown in Figure 3a. In general, when the WO_3 film was cathodically polarized in H_2SO_4, it became blue, and the color darkened with higher applied voltage. When the blue film was anodically polarized, it was bleached and became transparent again. To make a fully on-chip device that is feasible for modern applications, a polyelectrolyte was utilized instead of the H_2SO_4 solution. The structure design is shown in Figure S2 (Supporting Information). In situ transmittance spectra of the on-chip WO_3 film were recorded at −2.0 (colored) and +2.0 V (bleached), as shown in Figure 3b. As previously reported, the maximum transmittance of the WO_3 electrochromic film was observed at a wavelength of 632.8 nm.[16] An in situ switching test examining coloration/bleaching of the as-prepared WO_3 electrochromic film was carried out at 632.8 nm, as shown in Figure 3c. The maximum transmittance difference between coloration and bleaching is ≈15.1%, which is consistent with the results in Figure 3b. We define the coloration and bleaching time as the time needed to reach 90% of the full response. Then, as the inset of Figure 3c (an enlarged view of a single switching cycle) shows, the coloration and bleaching times are 2.3 and 8.9 s, respectively. The cyclic stabilities of the device are shown in Figure 3d, and over 85% of the color contrast was maintained after 300 cycles.

Coloration efficiency (CE) is another important parameter for ECDs. It is defined as

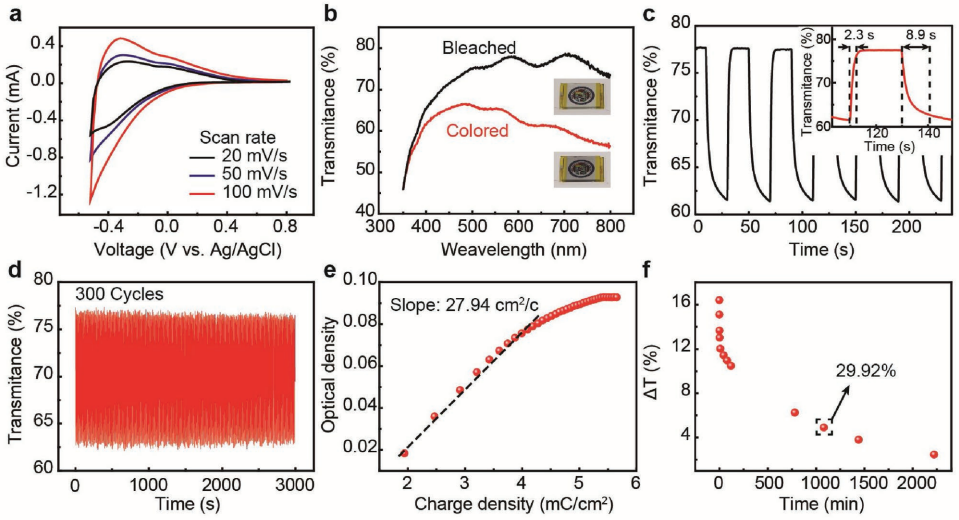

Figure 3. Performance of the WO_3 ECD. a) Cyclic voltammograms of the WO_3 thin film, cycled between –0.5 and 0.8 V in 1 M H_2SO_4 at different sweep rates of 20, 50, and 100 mV s^{-1}. b) The UV–vis spectra of the colored and bleached ECD with –2 V and +2 V voltage bias. c) The color switching behavior measured at 632.8 nm. Inset is a magnified view of a single switching cycle. d) Cyclic switching over 300 cycles. e) Optical-density–charge-density test at 632.8 nm. The CE value was measured to be 27.94 cm^2 C^{-1}. f) The color retention ability test measuring transmittance at 632.8 nm.

$$CE = \frac{OD}{Q/A} = \log\left(\frac{T_b}{T_c}\right)/(Q/A) \quad (2)$$

where OD is the optical density, Q is the charge, A is the electrode area, and T_b and T_c stand for the transmittance of the ECD in the bleached and colored states, respectively. A high CE value means that we can change the color (transmittance) with low electrical charge or under low polarizing voltage.[17] Figure 3e shows the relationship between the optical density and the intercalation charge density in the coloring process at 632.8 nm. By fitting a line to the linear region of the optical-density–charge-density curve, the CE value can be found from the slope of the fitting line, and here, it was measured to be 27.94 cm^2 C^{-1}, as shown in Figure 3e. The color retention ability was also carefully investigated, as shown in Figure 3f. The transmittance dropped sharply after removing the power supply and remained unchanged for a long time. The color of the WO_3 film was maintained over 37 h, and the transmittance remained at ≈29.92% after 18 h. This is the so-called "color memory effect".

Based on the above investigations, the color of the pixel in the ECD can be changed by piezoelectric charges from corresponding pixels in the ZPS matrix, which are related to the applied pressure. **Figure 4**a schematically illustrates the experimental setup, and further details can be found in the Experimental Section. The pixels in the ZPS component are compressed by the pressure-induced piezoelectric charges, and these charges can change the color of the corresponding pixels in the ECD array, which are connected by the middle electrode layer, while the color of the other pixels in the ECD array that are connected to uncompressed pixels remain unchanged. Therefore, applied pressure on the ZPS component can be visualized through the color change of pixels in the ECD array. Figure 4b shows the RGB map of all 100 pixels in their initial state. All 100 pixels can be colored by a –2 V voltage (left) and can be bleached to their initial state by a +2 V voltage. The 2D pressure visualization is demonstrated using a convex "E"-patterned stamp. Each red dot in Figure 4c represents a pixel in the ECD array, and Figure 4d–f shows the pressure visualization performance under pressures of 0, 72.12, and 120.20 MPa at –1 V. The RGB maps clearly show the enhancement of the pixels compressed by the 'E' pattern. The "pressure map" can be retained for a period of time through the color memory effect. To better illustrate the modulation results from the piezotronic effect, we introduce an enhancement factor E, which is defined as $E = (\Sigma rgb^{\varepsilon} - \Sigma rgb^{0})/\Sigma rgb^{0}$, where Σrgb^{0} and Σrgb^{ε} represent the RGB values in the strain-free and stressed conditions, respectively. The E factor of a certain pixel was investigated. As the applied pressure increased from 0 to 120.20 MPa, the E factor increased linearly from 0 to 900%, and the corresponding picture is presented in Figure 4g.

In conclusion, we fabricated a PVR system by integrating a piezotronic ZPS and a WO_3-film ECD array (10 × 10 pixels). Each pixel of the ECD array is connected to a specific bunch of ZnO nanowires in the ZPS component. The WO_3-film ECD demonstrated good cyclic stability and maintained over 85% of its color contrast after 300 cycles. Using this PVR system, the distribution of external pressure can be directly visualized by color changes and recorded on the ECD section without the assistance of a computer, due to the color memory effect of the WO_3 material. The PVR system may have applications in human-electronic interfaces, military applications, and smart robots.

Experimental Section

Preparation of WO_3 Film (Electrochromic Layer): The WO_3 film was prepared using RF magnetron sputtering (Kurt J. Lesker PVD75) under the conditions of 30:20 O_2:Ar, 2 Pa sputtering pressure, 120 W power, and 60 min time. The sputtering target was tungsten oxide with a purity

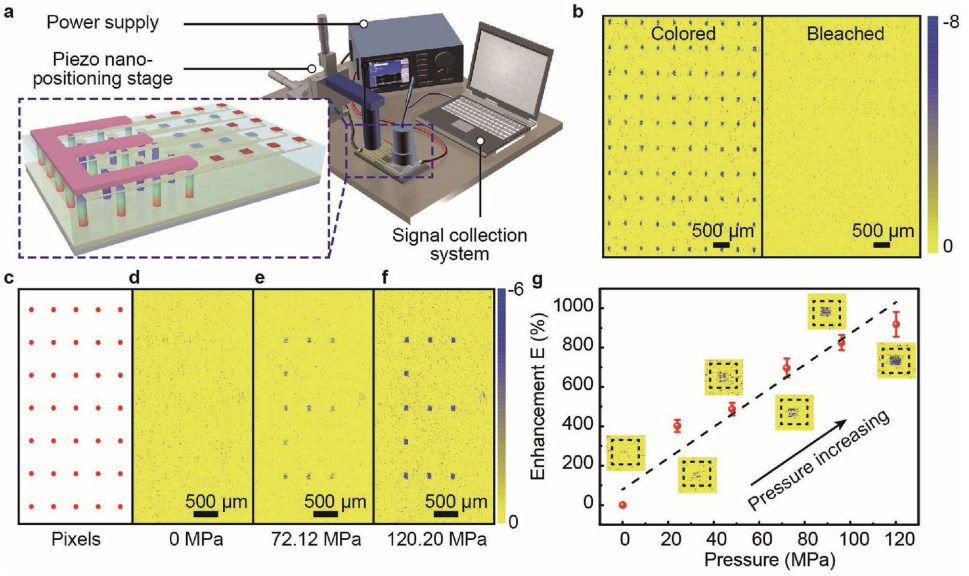

Figure 4. Pressure visualization performance of the integrated PVR system. a) Experiment setup to measure the pressure visualization and recording abilities. b) RGB map of the 10 × 10 pixel array in the colored and bleached states without applied pressure. c) Pixel distribution in the sensing area. RGB maps of an "E"-patterned stamp under different pressures of d) 0, e) 72.12, and f) 120.20 MPa. g) Enhancement factor *E* versus applied pressure, with corresponding RGB images of a single pixel.

of 99.99%. The thickness of the film, as measured by a profilometer (KLA-Tencor), was ≈100 nm.

Preparation of Polyelectrolyte: $LiClO_4{\cdot}3H_2O$ was evaporated in a vacuum drying oven at 120 °C for 2 h and then dissolved in propylene carbonate to obtain a 1 M solution. Subsequently, 25 wt% poly(methyl methacrylate) was mixed into the as-prepared solution and stirred at 100 °C for 12 h.

Fabrication of the PVR system: A 3 cm × 2 cm glass, 1 mm in thickness, was ultrasonically cleaned by alcohol, isopropyl, and deionized water in sequence and then dried in air for 2 h for use as the device substrate. First, a layer of ITO was deposited as the bottom electrode by RF magnetron sputtering (Kurt J. Lesker PVD75). Second, patterned Au (20 nm) and ZnO (100 nm) layers were sequentially deposited with dimensions of 20 μm × 20 μm and spacings of 480 μm by RF magnetron sputtering (Kurt J. Lesker PVD75). Third, the as-deposited substrate with the patterned ZnO seed layer was placed into a nutrient solution containing 20×10^{-3} M zinc nitride (Alfa Aesar) and 20×10^{-3} M hexamethylenetetramine (Fluka) in an oven at 90 °C for 6 h to synthesize ZnO NWs. Fourth, a layer of SU-8 photoresist was spin-coated, followed by post-baking at 135 °C for 2 h. Oxygen plasma cleaning was then applied to etch the top part of the photoresist and expose the tips of the ZnO NWs. Fifth, a patterned Au (20 nm) layer and an ITO (150 nm) layer as the middle electrode were deposited by RF magnetron sputtering (Kurt J. Lesker PVD75). Sixth, a patterned WO_3 layer (100 nm) was deposited with a dimension of 80 μm × 80 μm and spacing of 420 μm to match the resolution of the ZnO nanowire array. Finally, the polyelectrolyte was dropped on the as-fabricated WO_3 film array, a piece of 2 cm × 1 cm ITO glass was placed on top as the top electrode, and the two parts were held together and heated at 100 °C for 10 min to form a sandwich-type device.

Experimental Setup and Measurements: The measurement system was customized based on two piezo nanopositioning stages (Newport M-462) with a closed-loop resolution of 0.2 nm, an electronic dynamometer (ATI Nano25), a power supply (Tektronix AFG3011C) and an image capture system. The *I–V* and *I–t* curves from a single pixel were obtained using a semiconductor test system (Keithley 4200). Cyclic voltammograms were measured using a three-electrode system with Pt wire as the counter electrode and Ag/AgCl as the reference electrode in 1 M H_2SO_4 electrolyte using an electrochemical workstation (Autolab). In situ transmittance spectra were obtained using a four-layer ECD with ITO glass as the bottom and top electrodes, the WO_3 film as the electrochromic layer and the polyelectrolyte as the cation transport layer using a UV–vis spectrophotometer (Shimadzu UV-3600). A normal force/pressure was applied on the top surface of the ZnO nanowire array using a glass substrate controlled by the piezoelectric nanopositioning stage. The pressure was recorded by an electronic dynamometer.

Supporting Information

Supporting Information is available from the Wiley Online Library or from the author.

Acknowledgements

The authors are thankful for support from the "Thousand Talents" program of China for pioneering researchers and innovative teams and from the President Funding of the Chinese Academy of Sciences, National Natural Science Foundation of China (Nos. 51432005, 61405040, 61505010, and 51502018), Beijing City Committee of science and technology (Z151100003315010), Beijing Natural Science Foundation (2164077 and 2164076).

Conflict of Interest

The authors declare no conflict of interest.

Keywords

electrochromic devices, piezotronic effect, pressure visualization, pressure recording, ZnO nanowire arrays

Received: March 5, 2017
Revised: March 29, 2017
Published online: May 3, 2017

[1] a) V. Maheshwari, R. F. Saraf, *Angew. Chem., Int. Ed.* **2008**, *47*, 7808; b) M. L. Hammock, A. Chortos, B. C. K. Tee, J. B. H. Tok, Z. A. Bao, *Adv. Mater.* **2013**, *25*, 5997; c) S. Jung, J. H. Kim, J. Kim, S. Choi, J. Lee, I. Park, T. Hyeon, D. H. Kim, *Adv. Mater.* **2014**, *26*, 4825; d) C. F. Pan, L. Dong, G. Zhu, S. M. Niu, R. M. Yu, Q. Yang, Y. Liu, Z. L. Wang, *Nat. Photonics* **2013**, *7*, 752; e) X. D. Wang, L. Dong, H. L. Zhang, R. M. Yu, C. F. Pan, Z. L. Wang, *Adv. Sci.* **2015**, *2*, 1500169.

[2] W. Gao, S. Emaminejad, H. Y. Y. Nyein, S. Challa, K. V. Chen, A. Peck, H. M. Fahad, H. Ota, H. Shiraki, D. Kiriya, D. H. Lien, G. A. Brooks, R. W. Davis, A. Javey, *Nature* **2016**, *529*, 509.

[3] N. S. Lu, D. H. Kim, *Soft Rob.* **2014**, *1*, 53.

[4] a) T. Someya, Y. Kato, T. Sekitani, S. Iba, Y. Noguchi, Y. Murase, H. Kawaguchi, T. Sakurai, *Proc. Natl. Acad. Sci. USA* **2005**, *102*, 12321; b) Y. P. Zang, F. J. Zhang, C. A. Di, D. B. Zhu, *Mater. Horiz.* **2015**, *2*, 140.

[5] a) B. Crone, A. Dodabalapur, Y. Y. Lin, R. W. Filas, Z. Bao, A. LaDuca, R. Sarpeshkar, H. E. Katz, W. Li, *Nature* **2000**, *403*, 521; b) J. Park, Y. Lee, J. Hong, Y. Lee, M. Ha, Y. Jung, H. Lim, S. Y. Kim, H. Ko, *ACS Nano* **2014**, *8*, 12020; c) X. L. Zhao, Q. L. Hua, R. M. Yu, Y. Zhang, C. F. Pan, *Adv. Electron. Mater.* **2015**, *1*, 201500142.

[6] a) X. D. Wang, H. L. Zhang, L. Dong, X. Han, W. M. Du, J. Y. Zhai, C. F. Pan, Z. L. Wang, *Adv. Mater.* **2016**, *28*, 2896; b) W. Z. Wu, X. N. Wen, Z. L. Wang, *Science* **2013**, *340*, 952; c) C. Pang, G. Y. Lee, T. I. Kim, S. M. Kim, H. N. Kim, S. H. Ahn, K. Y. Suh, *Nat. Mater.* **2012**, *11*, 795; d) T. Yamada, Y. Hayamizu, Y. Yamamoto, Y. Yomogida, A. Izadi-Najafabadi, D. N. Futaba, K. Hata, *Nat. Nanotechnol.* **2011**, *6*, 296; e) M. X. Chen, C. F. Pan, T. P. Zhang, X. Y. Li, R. R. Liang, Z. L. Wang, *ACS Nano* **2016**, *10*, 6074; f) Q. L. Liao, M. Mohr, X. H. Zhang, Z. Zhang, Y. Zhang, H. J. Fecht, *Nanoscale* **2013**, *5*, 12350.

[7] a) X. D. Wang, H. L. Zhang, R. M. Yu, L. Dong, D. F. Peng, A. H. Zhang, Y. Zhang, H. Liu, C. F. Pan, Z. L. Wang, *Adv. Mater.* **2015**, *27*, 2324; b) C. Wang, D. Hwang, Z. B. Yu, K. Takei, J. Park, T. Chen, B. W. Ma, A. Javey, *Nat. Mater.* **2013**, *12*, 899; c) X. Y. Li, M. X. Chen, R. M. Yu, T. P. Zhang, D. S. Song, R. R. Liang, Q. L. Zhang, S. B. Cheng, L. Dong, A. L. Pan, Z. L. Wang, J. Zhu, C. F. Pan, *Adv. Mater.* **2015**, *27*, 4447; d) X. Q. Liao, Q. L. Liao, Z. Zhang, X. Q. Yan, Q. J. Liang, Q. Y. Wang, M. H. Li, Y. Zhang, *Adv. Funct. Mater.* **2016**, *26*, 3074.

[8] a) H. H. Chou, A. Nguyen, A. Chortos, J. W. F. To, C. Lu, J. G. Mei, T. Kurosawa, W. G. Bae, J. B. H. Tok, Z. A. Bao, *Nat. Commun.* **2015**, *6*, 8011; b) Y. H. Sun, X. Q. Yan, X. Zheng, Y. C. Liu, Y. W. Shen, Y. Zhang, *Nano Res.* **2016**, *9*, 1116.

[9] P. R. Somani, S. Radhakrishnan, *Mater. Chem. Phys.* **2003**, *77*, 117.

[10] a) Y. Zhang, X. Q. Yan, Y. Yang, Y. H. Huang, Q. L. Liao, J. J. Qi, *Adv. Mater.* **2012**, *24*, 4647; b) Q. L. Liao, M. Y. Liang, Z. Zhang, G. J. Zhang, Y. Zhang, *Nano Res.* **2015**, *8*, 3772.

[11] a) X. Han, W. M. Du, R. M. Yu, C. F. Pan, Z. L. Wang, *Adv. Mater.* **2015**, *27*, 7963; b) Z. M. Bai, X. Q. Yan, X. Chen, H. S. Liu, Y. W. Shen, Y. Zhang, *Curr. Appl. Phys.* **2013**, *13*, 165.

[12] Z. L. Wang, *Adv. Mater.* **2012**, *24*, 4632.

[13] a) D. S. Dalavi, R. S. Devan, R. A. Patil, R. S. Patil, Y. R. Ma, S. B. Sadale, I. Kim, J. H. Kim, P. S. Patil, *J. Mater. Chem. C* **2013**, *1*, 3722; b) P. K. Shen, A. C. C. Tseung, *J. Mater. Chem.* **1992**, *2*, 1141.

[14] a) B. Orel, U. O. Krasovec, U. L. Stangar, P. Judeinstein, *J. Sol-Gel Sci. Technol.* **1998**, *11*, 87; b) J. S. E. M. Svensson, C. G. Granqvist, *Sol. Energy Mater.* **1985**, *12*, 391; c) K. J. Patel, C. J. Panchal, M. S. Desai, P. K. Mehta, *Mater. Chem. Phys.* **2010**, *124*, 884.

[15] a) H. H. Lu, *J. Alloys Compd.* **2008**, *465*, 429; b) J. Z. Ou, S. Balendhran, M. R. Field, D. G. McCulloch, A. S. Zoolfakar, R. A. Rani, S. Zhuiykov, A. P. O'Mullane, K. Kalantar-zadeh, *Nanoscale* **2012**, *4*, 5980.

[16] a) D. Y. Ma, G. Y. Shi, H. Z. Wang, Q. H. Zhang, Y. G. Li, *J. Mater. Chem. A* **2013**, *1*, 684; b) J. M. Wang, E. Khoo, P. S. Lee, J. Ma, *J. Phys. Chem. C* **2009**, *113*, 9655.

[17] C. Y. Yan, W. B. Kang, J. X. Wang, M. Q. Cui, X. Wang, C. Y. Foo, K. J. Chee, P. S. Lee, *ACS Nano* **2014**, *8*, 316.

